Microstructural Effects on High-Cycle Fatigue-Crack Initiation in A356.2 Casting Alloy

B. ZHANG, D.R. POIRIER, and W. CHEN

The effects of various microconstituents on crack initiation and propagation in high-cycle fatigue (HCF) were investigated in an aluminum casting alloy (A356.2). Fatigue cracking was induced in both axial and bending loading conditions at strain/stress ratios of −1, 0.1, and 0.2. The secondary dendrite arm spacing (SDAS) and porosity (maximum size and density distribution) were quantified in the directionally solidified casting alloy. Using scanning electron microscopy, we observed that cracks initiate at near-surface porosity, at oxides, and within the eutectic microconstituents, depending on the SDAS. When the SDAS is greater than ~ 25 to 28 μm, the fatigue cracks initiate from surface and subsurface porosity. When the SDAS is less than ~ 25 to 28 μm, the fatigue cracks initiate from the interdendritic eutectic constituents, where the silicon particles are segregated. Fatigue cracks initiated at oxide inclusions whenever they were near the surface, regardless of the SDAS. The fatigue life of a specimen whose crack initiated at a large eutectic constituent was about equal to that when the crack initiated at a pore or oxide of comparable size.

I. INTRODUCTION

THE mechanical properties of widely used A356.2 aluminum castings have been related to microstructural features such as secondary dendrite arm spacing (SDAS),[1,2,3] microporosity,[4,5,6] intermetallics,[7] and eutectic silicon particles[8,9] and to variations in heat treatment[10,11] since the late 1940s. Although the study of the relationship between fatigue properties and microstructures in A356 can be dated back to the 1950s,[12] it has been only recently that there has been a concerted impetus to use more aluminum castings in automobiles[13,14] to achieve weight reduction and corresponding improvements in fuel economy and emissions. As sound commercial aluminum castings find more applications, more information on the effects of microstructures on fatigue properties would enhance both the practical improvement of the current casting processing and the fundamental understanding of fatigue processes in aluminum casting alloys.

It is generally accepted that the fatigue process consists mainly of four important stages: microcrack initiation, microcrack coalescence and growth (small-crack propagation), macrocrack growth, and final fracture. From the point view of fatigue life, the crack propagation dominates the low-cycle fatigue (LCF) life, and crack initiation controls the high-cycle fatigue (HCF) life. Fatigue cracks in aluminum alloys have been found to initiate from slip bands, constituent particle breakage and debonding, and grain-boundary separation.[15] In hypoeutectic Al-Si casting alloys, fatigue cracks usually initiate from shrinkage pores at or close to the specimen surface,[16–23] often associated with a small crack-initiation period.[23] However, research has been focused on fatigue-crack propagation of long cracks using linearly elastic fracture-mechanics methods. Much more research on small-crack propagation[24] in commercial aluminum castings is needed to better reveal the interaction of microstructures with the fatigue process.

In this study, we investigated microstructural effects on HCF crack initiation and the interaction of microstructure with the propagation of fatigue cracks during HCF in A356.2 specimens removed from a casting ingot with gradients in SDAS and porosity. In related work,[25] the fatigue lives of the specimens are given for both LCF and HCF conditions, without the level of detail on microconstituents presented here.

II. EXPERIMENTAL PROCEDURES

A. *Materials and Fatigue Testing*

The A356.2 casting ingots were solidified with bottom-water cooling to effect a gradient in SDAS. The melt was degassed with Ar, grain refined with an Al-3Ti-1B master alloy, and modified with an Al-15Sr alloy. The composition (in wt pct) was 6.87 Si, 0.36 Mg, 0.03 Fe, 0.10 Ti, 0.006 Sr, 0.01 Cu, less than 0.001 B, and the balance Al. Additional details can be found elsewhere.[23,26,27] After the castings were cut into slices for the fatigue specimens, the slices were heat treated to the T6 condition. The specimen geometry used in axial fatigue testing was from ASTM E466-82.[28] The bending-fatigue specimen geometry was determined by a finite-element stress analysis and several trial fatigue tests, to ensure a uniform strain distribution in the gage section.[23]

B. *Microstructural Characterization and Fatigue Fracture Observations*

Using light microscopy, the line-intercept method[2,3] was applied to measure the SDAS on samples removed from the as-cast ingots. Failed fatigue samples, which contained main and small cracks, were examined using either light microscopy or scanning electron microscopy (SEM) to investigate the interaction between the fatigue cracks and the contiguous microstructures. Examination at finer scales was conducted

B. ZHANG, Graduate Research Assistant, and D.R. POIRIER, Professor, Department of Materials Science and Engineering, and W. CHEN, Assistant Professor, Department of Aerospace and Mechanical Engineering, are with The University of Arizona, Tucson, AZ 85721.

Manuscript submitted December 29, 1998.

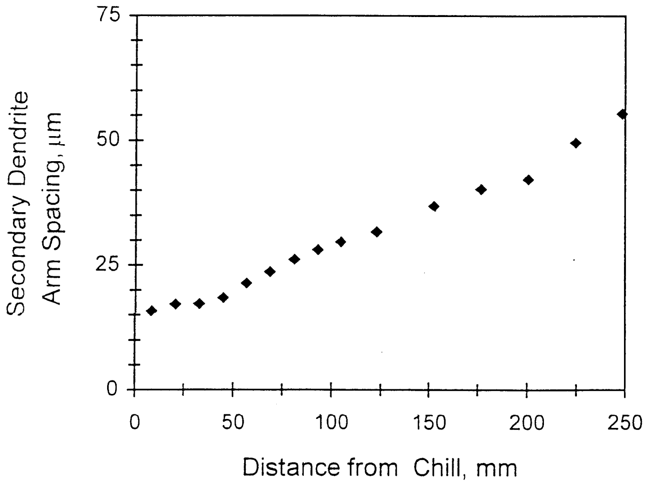

Fig. 1—Variation of SDAS along ingot height.

using SEM, which revealed the fatigue-crack initiation sites, propagation paths, fracture modes, *etc.*

C. *Number Density of Pores and Maximum Pore Size*

Radiographs were made before mechanical testing to reveal the porosity (maximum size and number density) in the fatigue specimens removed from the bottom to the top of the ingots. A radiography unit with a tungsten target of an effective focal spot of 2.0 mm was used. Pores visible on the radiographs at a magnification of 20 times were counted within a grid of an area of 34.10 mm^2 (5.84 $\times$ 5.84 mm). The number of pores in a total of 12 grid areas within the gage section of each specimen was counted, and then the number density was averaged. The size of the largest pore, determined at a magnification of 20 times in each specimen, was further measured at a magnification of 38.75 times.

D. *Area and Maximum Size of Crack-Initiation Sites on Fractures*

The fatigue-crack initiation sites on the fatigue fractures were identified with the aid of either a light microscope or SEM, depending on the size of the sites. Both the maximum size and the area of the projection of the initiation sites (porosity, oxide inclusions, and eutectic constituents) were measured. A grid with an area of 2.117 mm^2 (1.455 $\times$ 1.455 mm) was used for area measurement on photomicrographs. Only the crack-initiation site that caused the fatal fatigue crack was measured when multiple crack-initiation sites were found.

III. RESULTS AND DISCUSSIONS

A. *The Variation of SDAS along the Height of the Ingot*

Figure 1 shows the variation of SDAS along the ingot height, measured upward from the bottom chill. Below a distance of 50 mm from the bottom chill, the SDAS increases slightly from 15 to 20 μm as the height increases. Twenty seconds after pouring, a bottom plate was pulled so that the casting butt was exposed to direct water impingement. Thus, the variation in SDAS shows a change in slope at about 40 mm from the chilled surface, in Figure 1. Beyond that point, the SDAS increases almost linearly from 20 to 60 μm at 250 mm. According to a relationship cited by Spear and Gardner[1] on SDAS as a function of cooling rate in solidification, the calculated cooling rate varies from 17 K s^{-1} at the bottom of the casting ingot to 0.4 K s^{-1} at 250 mm from the bottom.

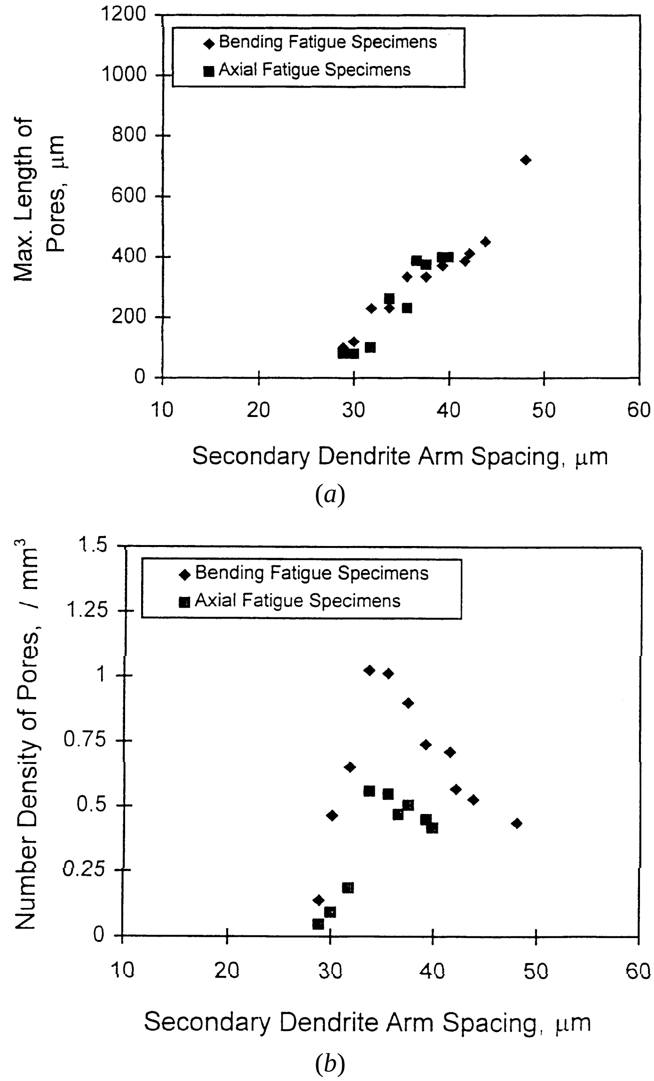

Fig. 2—Pores detected by radiography in the casting ingots (*a*) variation of maximum length and (*b*) number density of visible pores.

B. *Porosity Distribution as a Function of SDAS*

The variations of maximum length and density of porosity, visible on radiographs of the fatigue specimens (3-mm thick) with different SDASs, are summarized in Figures 2(a) and (b). The pores are obvious when the SDAS $>$ 28 μm; no visible pores, for specimens with a SDAS $<$ 28 μm, could be detected even under a magnification of 38.75 times. As the SDAS increases from 28 to 48 μm, the images of the pores become clearer, and the maximum length increases from about 0.08 mm (80 μm) to 0.7 mm (Figure 2(a)). Using this radiographic technique, no pores were detected in specimens that have an SDAS less than 28 μm. Figure 2(b) shows that the number density of visible pores is between approximately 0.4 to 1.1 mm^{-3} for most of the specimens, with four of the number densities less than 0.2 mm^{-3}, grouped at a SDAS of approximately 30 μm.

Although radiography did not detect the pores at the smaller SDAS, using metallographic techniques, Fang and Granger[27] found pores which were 50 to 25 μm in equivalent diameter for SDASs from 30 to 16 μm, in a grain-refined and modified A356.2, which was cast in the same manner as the ingots studied herein. However, pores of such small sizes are not active in terms of crack initiation, which takes place at eutectic microconstituents of larger sizes, as is discussed later. Results in Figure 2(a) show that, as the SDAS increases (cooling rate decreases), the maximum length of the pores increases, but, when the SDAS is greater than about 34 μm, the visible pore density decreases. These results are in agreement with the results from Tynelius *et al.*[29] and Shivkumar *et al.*,[30] where it was found that the maximum porosity area increases as the SDAS increases, and that, when the hydrogen content is above 0.22 mL/100 g in the alloy, the areal pore density decreases as the SDAS increases.

C. *Fatigue-Crack Initiation at Near-Surface Porosity*

Porosity has been widely reported to be the major initiation site for fatigue cracks in casting alloys. In this study, detailed observations of the fracture surfaces of the bending- and axial-fatigue specimens revealed other types of initiation sites in addition to pores, depending on the SDAS and microconstituents.

Although most of the initiation sites are at the surface, cracks initiated from subsurface porosity in a few of the bending-fatigue specimens. Subsurface crack initiation, related to preexisting defects and microcracks, has been reported in HCF at lower stresses for high-strength alloys.[31,32] The possibility that a subsurface pore or other defect can initiate a crack depends not only on its size, but also on its distance from the surface. The pore in Figure 3(a) is approximately 360 μm in length, and its closest distance to the surface is about 33 μm. Figure 3(b) shows the maximum lengths of subsurface defects that initiated cracks and their distances from the surface. For the fractures resulting from axial fatigue testing, we did not find any cracks that initiated from a subsurface pore, perhaps because the number density of large pores in the axial specimens was significantly less than in the bending specimens (Figure 2(b)). We found only one crack, which initiated from a subsurface oxide inclusion (200 μm in size, located at 250 μm from the surface). Seniw *et al.*[33] used a reduced section in fatigue specimens to establish the relationship of fatigue life to pore-initiation size and the distance from the surface. They found that most of the initiation sites were subsurface pores. So, whether the fatigue crack initiates from a subsurface defect depends on the extent to which the maximum stress is localized, the pore size, and the pore number density.

D. *Crack Initiation at Oxides at or near the Surface*

Different types of oxides were found to initiate fatigue cracks in both axial- and bending-fatigue specimens. Oxides poured into molds with the melts are more deleterious to

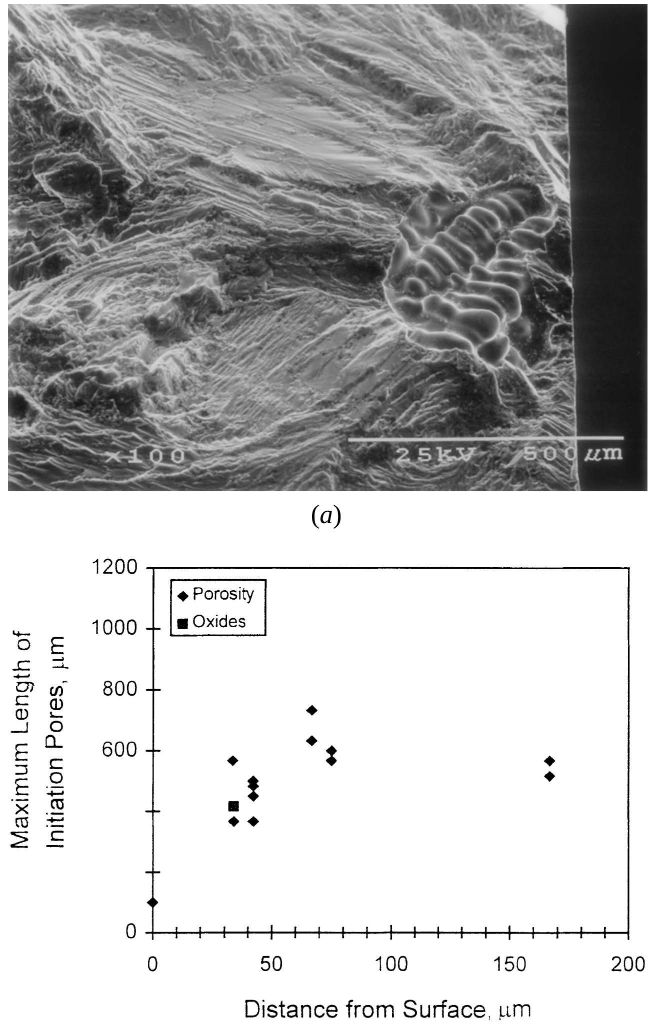

(*b*)

Fig. 3—Crack-initiation sites in bending fatigue specimens: (*a*) a near-surface pore, where the crack initiated in a specimen with a SDAS of 35 μm; and (*b*) distribution of crack-initiation sites in terms of their lengths and distances from surfaces.

fatigue properties. Figure 4(a) shows a crack-initiation site at an oxide which is about 75 μm from the surface of a specimen (SDAS = 25 μm). The energy-dispersive X-ray (EDX) analysis reveals the oxide to be $Al_xMg_yO_z$ (probably the spinel of Al_2O_3 and MgO or Al_2O_3 plus the spinel). On the surface of the oxide film, small particles (less than 5 μm) were detected, with different compositions: $Al_xMg_yO_z$, $Al_xSi_yO_z$, and Al_xC_y (possibly Al_4C_3). Its shape and higher Mg content indicate that it is an "old" oxide, which existed in the melting ingot, as described by Campbell *et al.*[34] Another old oxide with Mg was observed on the fracture of an axial-fatigue specimen (Figure 4(b)). It consists of two layers of oxide films with small particles of $Al_xMg_yO_z$ (less Si, Sr, and Ti) sitting on the film.

The oxides are as deleterious to fatigue resistance as are the pores. The fatigue life of a bending specimen with a SDAS of 25 μm, whose crack initiated at an old oxide, is 100 times less than that for a similar specimen with a crack initiated from a eutectic constituent and is almost the same as that for a specimen with a crack initiated from a pore of 267 μm in maximum length. Campbell *et al.*[34] and Wang

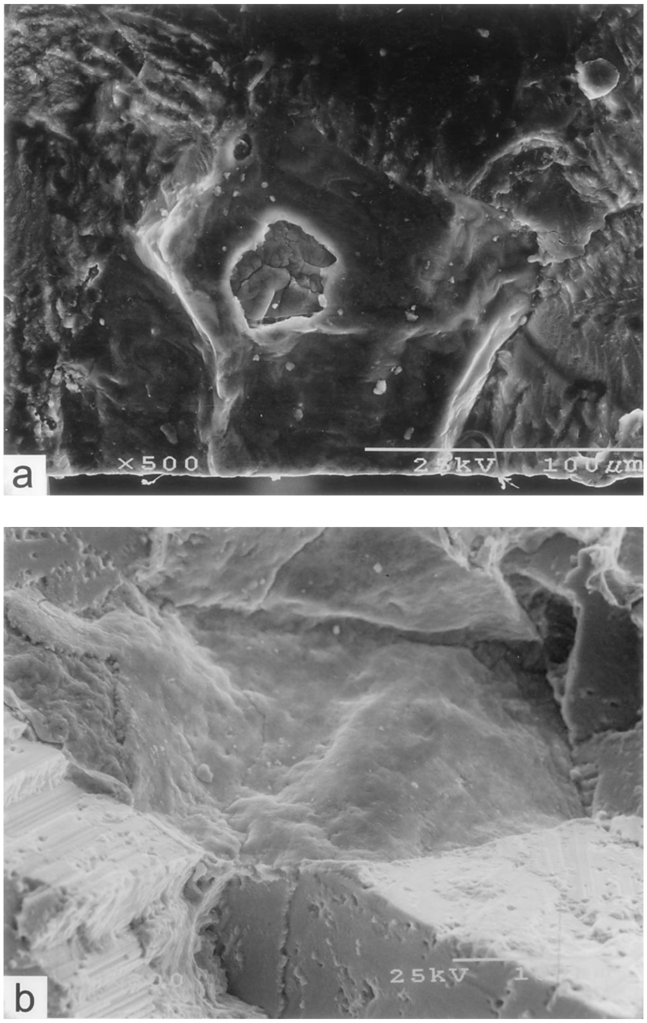

Fig. 4—Oxides revealed by SEM: (*a*) initiation site at subsurface oxide (SDAS = 25 μm, bending fatigue with maximum strain of 0.0016, $R = -1$, failed at 1.4×10^6 cycles); and (*b*) initiation site at an oxide film (SDAS = 17 μm, axial fatigue with maximum stress of 130 MPa, $R = 0.2$, failed at 5.0×10^6 cycles).

et al.[35] have stated that the fatigue cracks initiate from old or "new" oxides, and that the fatigue lives of most aluminum alloy castings could probably be improved by a factor of 100 to 10,000 times by a combination of attention to metal quality and casting technique.

Figure 5 shows a new oxide that developed on the surface of the molten alloy during pouring. This oxide initiated a fatigue crack in a specimen with a SDAS of 17 μm. Indication of debonding was seen on the other half of the fatigue fracture that is not shown here. The oxide consists of $Al_xSi_yO_z$ with only a very slight indication of Mg, in contrast to the old oxides, which showed clear indications of Mg. Smaller particles sitting on the film were detected, with qualitative compositions of $Al_xSi_yO_z$ and $Al_xC_ySi_z$. The fatigue life of this specimen was about the same as in specimens in which the eutectic constituent initiated cracks. It seems that the new oxide is not particularly deleterious, if it is not folded and aggregated.

New oxides formed during turbulent pouring were found in specimens near the bottom of the casting ingot, even though the mold was tilted during the pouring to minimize their formation. Figure 6(a) shows such an oxide film, which initiated the fatigue crack in a specimen with a SDAS of 16 μm. The film is Al_xO_y, with a small amount of Si and barely a trace of Mg. At a higher magnification, we found submicron particles of Al_xO_y (probably Al_2O_3) that decorated the surface of the films. These are the new oxides described by Campbell *et al.*[34] At a much lower magnification (Figure 6(b)), the oxide appears as folded films, which follow eutectic constituents for several SDASs.

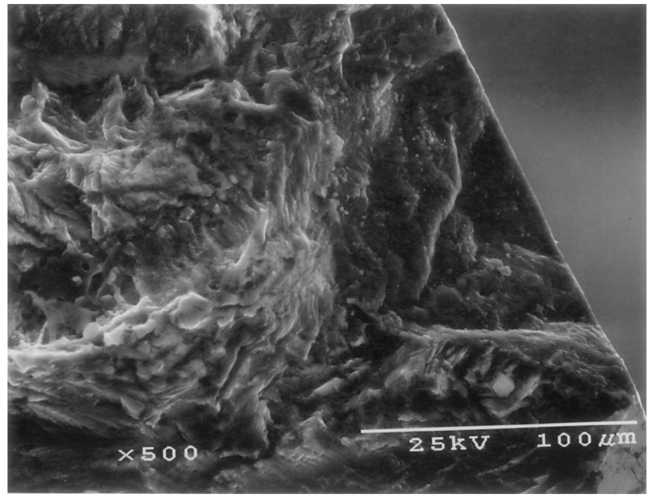

Fig. 5—Crack-initiation site at an oxide revealed by SEM (SDAS = 17 μm, axial fatigue with maximum stress of 175 MPa, $R = 0.1$, failed at 7.8×10^5 cycles).

E. *The HCF Crack Initiation at Eutectic Areas*

When the SDAS is less than 25 μm and no large oxide inclusions are present, HCF cracks initiate exclusively from the eutectic constituent. Figure 7 shows a portion of a rather large eutectic constituent (210 μm in maximum length), which initiated a fatigue crack at the surface. Many of the silicon particles in the eutectic constituent are debonded from the aluminum-rich phase; EDX analysis shows that, on the surface of a debonded silicon particle, there is a layer of aluminum. Well-organized marks left by the debonded silicon particles can also be seen in Figure 7, which indicated that the debonding was from a sliding mechanism.

Since the silicon particles in the interdendritic area are stiffer than the matrix,[30] then the stress has to be distributed in such a way that the clusters bear more load than the rest of the matrix to satisfy the deformation compatibility. Apparently, the stress concentration created in this area is enough to cause microslips in the matrix close to the silicon particles, which led to the particle debonding and then crack initiation. According to Lee *et al.*,[36] a Sr-modified eutectic alloy (Al-12 wt pct Si-0.35 wt pct Mg) showed better fatigue-crack growth resistance than the unmodified version of the alloy with coarse Si particles. Shiozawa *et al.*[24] investigated fatigue behavior in squeeze-cast aluminum alloys using smooth specimens subjected to rotary bending. Crack-initiation sites were at the silicon particles within the eutectic constituents at the surfaces of specimens. They suggested that an improvement in fatigue strength can be expected by refining the eutectic silicon rather than increasing the static strength.

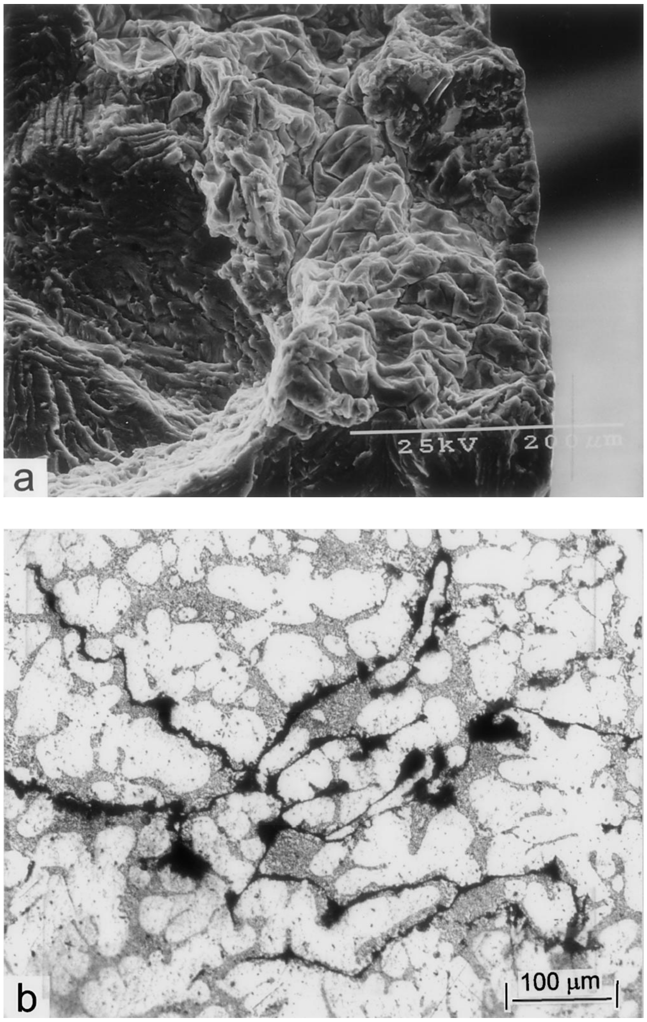

Fig. 6—New oxides: (*a*) initiation site at a folded oxide film (SDAS = 16 μm, axial fatigue with maximum stress of 175 MPa, $R = 0.1$, failed at 4.9×10^5 cycles); and (*b*) oxide films revealed by light microscopy (SDAS = 22 μm, as cast).

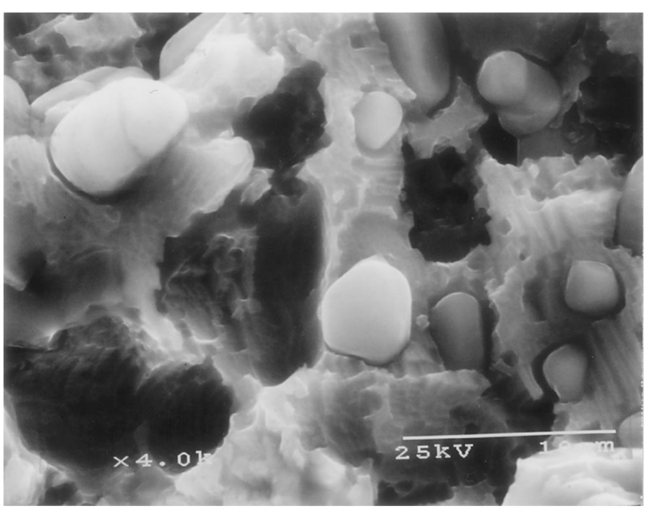

Fig. 7—Debonded Si particles in a crack-initiation site at an interdendritic eutectic constituent (SDAS = 29 μm, axial fatigue with maximum stress of 130 MPa, $R = 0.2$, failed at 1.5×10^5 cycles).

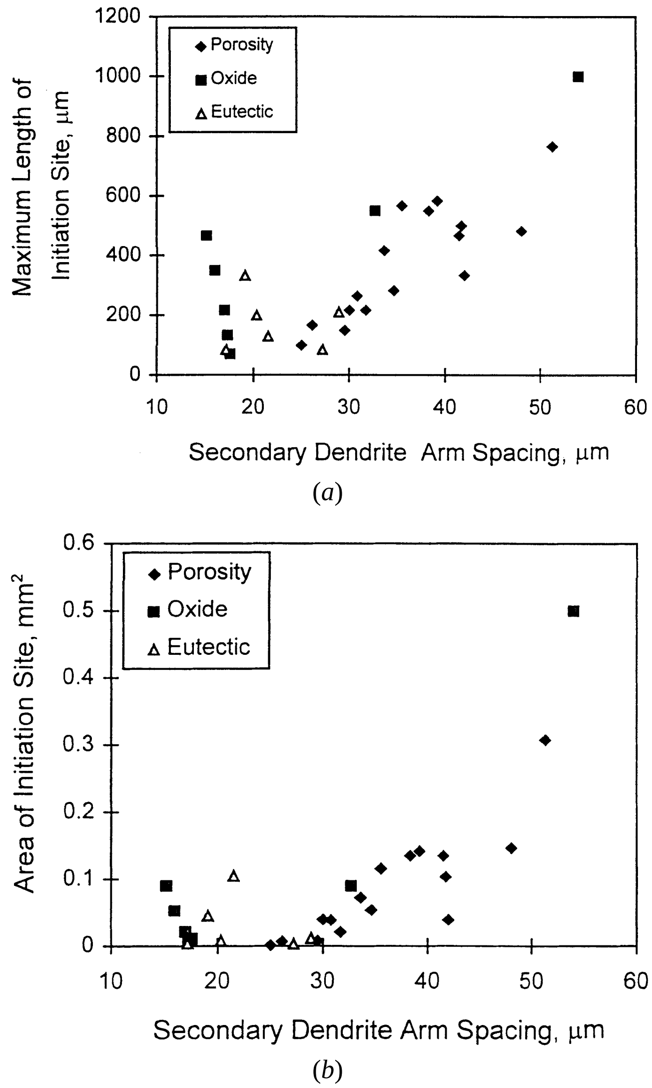

Fig. 8—Distribution of sizes of crack initiation sites in axial fatigue specimens: (*a*) maximum length and (*b*) area.

The size of a eutectic area was found to significantly affect the fatigue life. In a specimen with a SDAS of 22 μm, a fatigue crack initiated at a relatively small eutectic constituent of 100 μm in maximum length. The specimen exhibited the greatest life (2.49×10^7 cycles) among the bending-fatigue specimens with a stress/strain ratio (R) of -1, which is 30 times greater than that for a specimen with approximately the same SDAS but with an initiation site of a eutectic constituent of 417 μm in maximum length.

F. *Variation of Size of Crack-Initiation Site with SDAS*

The maximum size and area of the fatal fatigue-crack-initiation region was measured on each fatigue-tested specimen. Figures 8 and 9 show the size and area distribution as a function of SDAS for both the axial- and bending-fatigue testing, under $R = -1$, 0.1 and 0.2. Both the maximum length and the area distribution of the initiation site show the same trends in Figures 8 and 9. For discussion, we consider the maximum length. It should be noted that the pore lengths measured at the initiation sites on the fracture

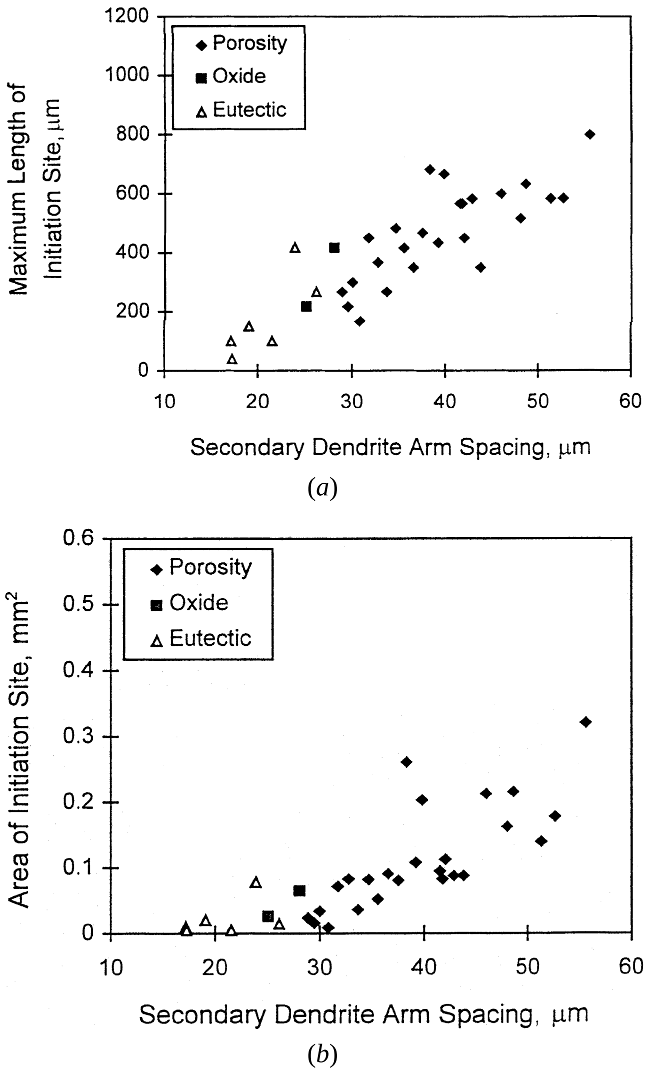

Fig. 9—Distribution of sizes of crack initiation sites in bending fatigue specimens: (*a*) maximum length and (*b*) area.

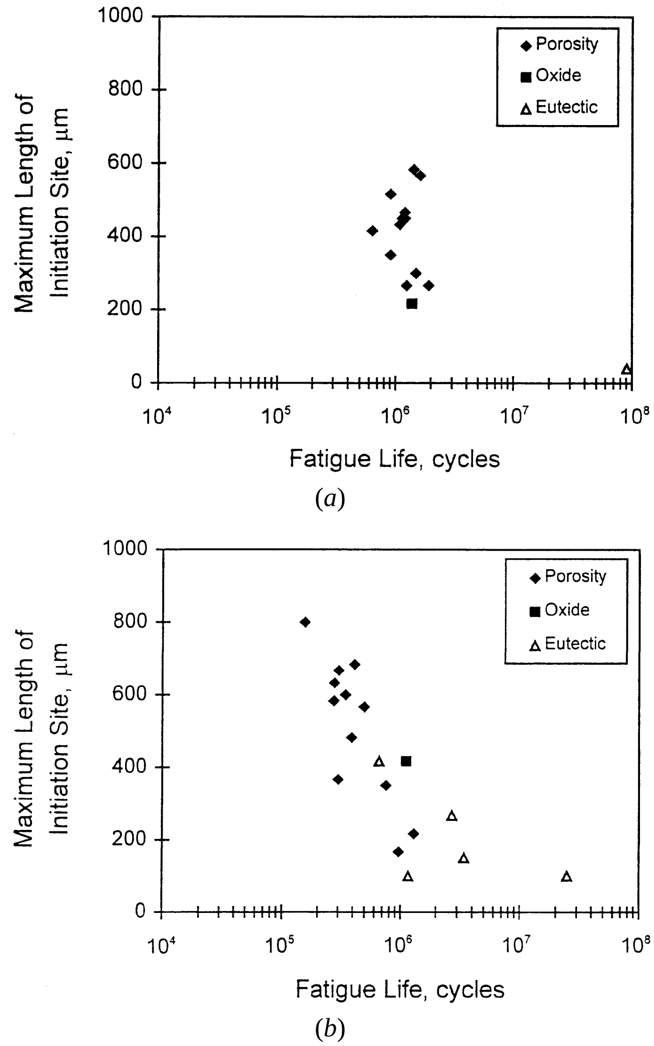

Fig. 10—Bending fatigue life as a function of maximum length of initiation site: (*a*) maximum strain = 0.0016, $R = 0.1$; and (*b*) maximum strain = 0.0016, $R = -1$.

surfaces were larger than the lengths detected on the radiographs (Figure 2(a)), due to much better resolution obtained by the SEM images of the fracture surfaces. When the SDAS is greater than ~25 to 28 µm, the cracks usually initiated at pores with lengths no smaller than 100 µm, for both axial and bending specimens. The lengths of the pores at the initiation sites increase as the SDAS increases, because the pores tend to increase in size as the SDAS increases (Figure 2(a)), when the SDAS is greater than 28 µm. All specimens that showed porosity on radiographs had relatively short fatigue lives.[25]

When the SDAS is less than ~25 to 28 µm, either oxide inclusions or eutectic constituents were found to be the sites of fatigue-crack initiation. If there is no oxide near the surface, then the eutectic constituent is the site of crack initiation. Five bending-fatigue specimens with SDASs below 28 µm had not broken after 2×10^7 cycles (maximum stress = 115 MPa, $R = 0.1$) when the tests were terminated. This may indicate an absence of oxide inclusions, eutectic constituents, and large pores as possible initiation sites. With the porosity in the alloy, it appears that its effect on initiating fatigue cracks overshadows the effect of the eutectic constituent, as shown in Figure 10(a) for high-cycle bending fatigue with $R = 0.1$. But for bending fatigue with $R = -1$ (Figure 10(b)), there is a tendency that the fatigue life decreases as the pore size increases. Sonsino and Ziese[19] also showed that, as the "degree of porosity" and maximum pore size increased, the fatigue strength decreased.

For axial HCF testing with $R = 0.1$ and -1 (Figures 11(a) and 11(b)), the fatigue life decreases as the pore or oxide size increases. Larger eutectic constituents also result in shorter fatigue life, although there are a few exceptions, as shown in Figures 10(b) and 11(b).

When the pore size is less than a critical size of about 100 µm, the eutectic constituent becomes the preferred initiation site, provided large oxides are absent. The larger the eutectic area, the lower the fatigue life, as a result of shorter initiation life. So, in addition to decreasing the pore size to below a critical size and eliminating oxides and oxide films in the melt, measures that would reduce the stress concentration within the eutectic constituent, such as a refinement of the size of the silicon particles and reduction of the aspect ratio of these particles, would increase fatigue life.

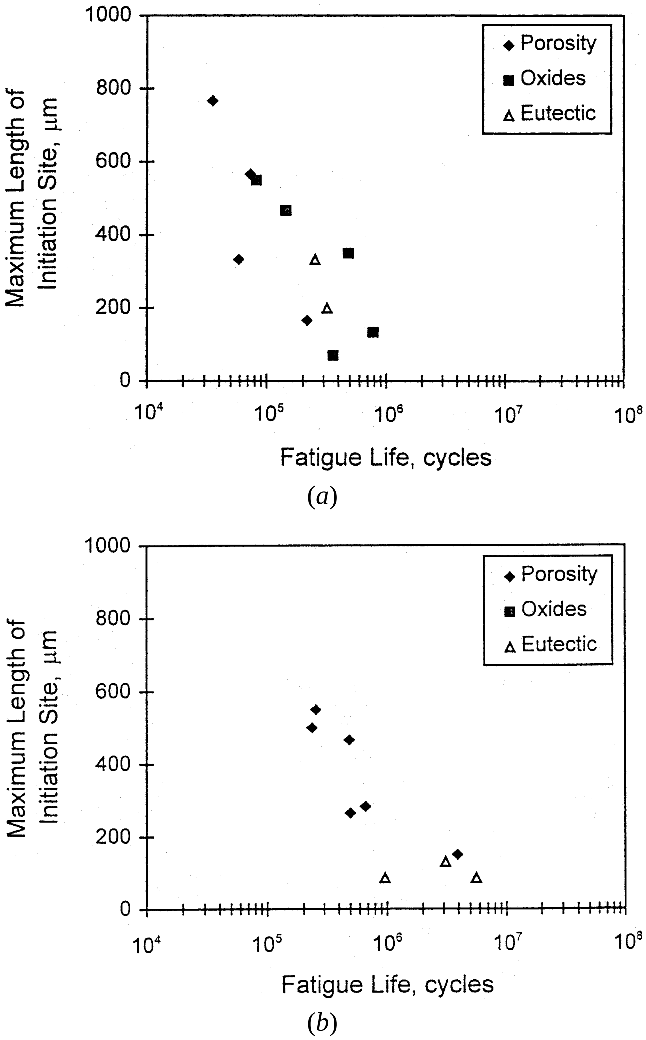

Fig. 11—Axial fatigue life as a function of maximum length of initiation site: (*a*) maximum stress = 175 MPa, $R = 0.1$; and (*b*) maximum stress = 85 MPa, $R = -1$.

IV. CONCLUSIONS

High-cycle fatigue-crack initiation and propagation in A356.2-T6 alloy, with a variety of SDASs and porosities, were investigated. The results show the following.

1. The HCF cracks initiate at porosity, oxides, or eutectic constituents, depending on the SDAS.
2. When the SDAS is greater than ~25 to 28 µm, the pores with a length greater than about 100 µm are the main crack-initiation sites. For HCF, the effect of SDAS is overshadowed by the effect of porosity on the fatigue life.
3. When the SDAS is below ~25 to 28 µm, the pore size is below the critical value, and large eutectic constituents initiate the HCF cracks. Large eutectic constituents result in a lower fatigue life than when that type of initiation site is smaller. Most of the silicon particles were debonded in the eutectic initiators of fatigue cracks.
4. The oxide defects initiate the fatigue crack when they are near or at the surface, regardless of SDAS. Old oxide films are more deleterious to fatigue life than the new oxide films.
5. Since fatigue cracks sometimes initiate at eutectic constituents in alloy A356.2, a refinement in the size and aspect ratio of the silicon particles would improve the resistance to the fatigue-crack initiation.

ACKNOWLEDGMENTS

The authors thank the United States Department of Energy for financial support. We also express our gratitude to Mr. G. Chandler, University of Arizona, for sharing his expertise in SEM with us, and to Professor L. Demer, for supervising the radiography and for being available to discuss SEM images. Dr. Q.T. Fang, Alcoa Technical Center, kindly supplied the casting ingots of A356 used in this study.

REFERENCES

1. R.E. Spear and G.R. Gardner: *AFS Trans.*, 1960, vol. 68, pp. 36-44.
2. K. Radhakrishna, S. Seshan, and M.R. Seshadri: *AFS Trans.*, 1980, vol. 88, pp. 695-702.
3. K.J. Oswalt and M.S. Misra: *AFS Int. Cast Met. J.*, 1981, vol. 6, pp. 23-40.
4. J. Eady and D.M. Smith: *Mater. Forum*, 1986, vol. 9, pp. 217-23.
5. M.K. Surappa, E. Blank, and J.C. Jaquet: *Scripta Metall.*, 1986, vol. 20, pp. 1281-86.
6. B. Closset and J.E. Gruzleski: *Metall. Trans. A*, 1982, vol. 13A, pp. 945-51.
7. G. Gustafsson, T. Thorvaldsson, and G.L. Dunlop: *Metall. Trans. A*, 1986, vol. 17A, pp. 45-52.
8. C.H. Caceres and J.R. Griffiths: *Acta Mater.*, 1996, vol. 44, pp. 25-33.
9. Q.G. Wang and C.H. Caceres: *Mater. Sci. Eng. A*, 1998, vol. 241A, pp. 72-82.
10. D.L. Zhang and L. Zheng: *Metall. Mater. Trans. A*, 1996, vol. 27A, pp. 3983-91.
11. C.H. Caceres and Q.G. Wang: *AFS Trans.*, 1996, vol. 104, pp. 1039-43.
12. W. A. Bailey: *Foundry*, 1965 (October), vol. 93 pp. 96-101.
13. J. Nath: SAE Technical Papers Series (SP-1097), No. 950723, SAE International, Warrendale, PA, 1995, pp. 75-90.
14. D. St John, C. Caceres, D. Zhang, and G. Edwards: *Mater. Aust.*, 1996 (April), vol. 28, pp. 14-16.
15. C.Y. Kung and M.E. Fine: *Metall. Trans. A*, 1979, vol. 10A, pp. 603-10.
16. M.J. Couper, A.E. Neeson, and J.R. Griffiths: *Fat. Fract. Eng. Mater. Struct.*, 1990, vol. 13, pp. 213-27.
17. J.C. Ting and F.V. Lawrence, Jr.: *Fat. Fract. Eng. Mater. Struct.*, 1993, vol. 16, pp. 631-49.
18. S. Gungor and L. Edwards: *Fat. Fract. Eng. Mater. Struct.*, 1993, vol. 16, pp. 391-403.
19. C.M. Sonsino and J. Ziese: *Int. J. Fat.*, 1993, vol. 15, pp. 75-83.
20. J.H. Elsner, E.P. Kvam, and A.F. Grandt, Jr.: *Metall. Mater. Trans. A*, 1997, vol. 28A, pp. 1157-67.
21. P.C. Inguanti: *Proc. 17th Nat. SAMPE Technical Conf.*, Kiamesha Lake, NY, Oct. 22–24, 1985, pp. 61-73.
22. J.M. Boileau, J.W. Zindel, and J.E. Allison: SAE Technical Papers Series (SP-1251), No. 970019, SAE International, Warrendale, PA, 1997, pp. 61-72.
23. W. Chen, B. Zhang. T. Wu, D.R. Poirier, P. Sung, and Q.T. Fang: in *Automotive Alloys II*, S.K. Das, ed., TMS, Warrendale, PA, 1998, pp. 99-113.
24. K. Shiozawa, Y. Tohda, and S.-M. Sun: *Fat. Fract. Eng. Mater. Struct.*, 1997, vol. 20, pp. 237-47.
25. W. Chen, B. Zhang, and D.R. Poirier: The University of Arizona, Tucson, AZ unpublished research, 1998.
26. Q.T. Fang and D.A. Granger: in *Light Metals 1989*, P.G. Campbell, ed., TMS, Warrendale, PA, 1989, pp. 927-35.
27. Q.T. Fang and D.A. Granger: *AFS Trans.*, 1989, vol. 97, pp. 989-1000.
28. “Standard Practice for Conducting Constant Amplitude Axial Fatigue Tests of Metallic Materials,” ASTM E466-82, *Annual Book of ASTM*

Standards, ASTM, Philadelphia, PA, 1982, vol. 03.01, pp. 465-69.
29. K. Tynelius, J.F. Major, and D. Apelian: *AFS Trans.*, 1993, vol. 101, pp. 401-13.
30. S. Shivkumar, L. Wang, and R. Lavigne: *Light Metals 1993*, S.K. Das, ed., TMS, Warrendale, PA, 1993, pp. 829-38.
31. H. Yokoyama, O. Umezawa, K. Nagai, and T. Suzuki: *Iron Steel Inst. Jpn. Int.*, 1997, vol. 37, pp. 1237-44.
32. O. Umezawa and K. Nagai: *Iron Steel Inst. Jpn. Int.*, 1997, vol. 37, pp. 1170-79.
33. M.E. Seniw, M.E. Fine, E.Y. Chen, M. Meshii, and J. Gray: in *High Cycle Fatigue of Structural Materials*, W.O. Soboyejo and T.S. Srivatsan, eds., TMS, Warrendale, PA, 1997, pp. 371-79.
34. J. Campbell, C. Nyahumwa, and N.R. Green: in *Advances in Aluminum Casting Technology*, M. Tiryakioglu and J. Campbell, eds., ASM INTERNATIONAL, Materials Park, OH, 1998, pp. 225-34.
35. Q.G. Wang, D. Apelian, and J.R. Griffiths: in *Advances in Aluminum Casting Technology*, M. Tiryakioglu and J. Campbell, eds., ASM INTERNATIONAL, Materials Park, OH, 1998, pp. 217-24.
36. F.T. Lee, J.F. Major, and F.H. Samuel: *Metall. Mater. Trans. A*, 1995, vol. 26A, pp. 1553-70.